LETTER • OPEN ACCESS

Limited role of climate change in extreme low rainfall associated with southern Madagascar food insecurity, 2019–21

To cite this article: Luke J Harrington *et al* 2022 *Environ. Res.: Climate* **1** 021003

View the article online for updates and enhancements.

ENVIRONMENTAL RESEARCH
CLIMATE

LETTER

Limited role of climate change in extreme low rainfall associated with southern Madagascar food insecurity, 2019–21

Luke J Harrington[1],* , Piotr Wolski[2], Izidine Pinto[2,8], Anzelà Mamiarisoa Ramarosandratana[3], Rondrotiana Barimalala[4,5] , Robert Vautard[6] , Sjoukje Philip[7], Sarah Kew[7], Roop Singh[8], Dorothy Heinrich[8], Julie Arrighi[8,9,10], Emmanuel Raju[11,12], Lisa Thalheimer[13] , Thierry Razanakoto[14], Maarten van Aalst[8,9,15], Sihan Li[16] , Remy Bonnet[6] , Wenchang Yang[17] , Friederike E L Otto[18] and Geert Jan van Oldenborgh[7,†]

1 Te Aka Mātuatua School of Science, University of Waikato, Hillcrest Road, Hamilton 3216, New Zealand
2 Climate System Analysis Group, University of Cape Town, Cape Town, South Africa
3 Direction des recherches et développement hydrométéorologiques", Direction Générale de la Météorologie', Antananarivo, Madagascar
4 Department of Oceanography, University of Cape Town, Cape Town, South Africa
5 NORCE Norwegian Research Centre, Jahnebakken 5, 5007 Bergen, Norway
6 Institut Pierre-Simon Laplace, CNRS, Sorbonne Université', Paris, France
7 Royal Netherlands Meteorological Institute (KNMI), De Bilt, The Netherlands
8 Red Cross Red Crescent Climate Centre, The Hague, The Netherlands
9 Faculty of Geo-Information Science and Earth Observation (ITC), University of Twente, Enschede, The Netherlands
10 Global Disaster Preparedness Center, American Red Cross, Washington, DC, United States of America
11 African Centre for Disaster Studies, Unit for Environmental Sciences and Management, North-West University, Potchefstroom, South Africa
12 Global Health Section, University of Copenhagen, Copenhagen, Denmark
13 Princeton School of Public and International Affairs, Princeton University, Princeton 08540, United States of America
14 Centre d'Etudes et de Recherches Economiques pour le Développement (CERED), Université d'Antananarivo, Antananarivo, Madagascar
15 International Research Institute for Climate and Society, Columbia University, New York, United States of America
16 School of Geography and the Environment, University of Oxford, Oxford, United Kingdom
17 Department of Geosciences, Princeton University, Princeton 08544, United States of America
18 Grantham Institute, Imperial College London, London, United Kingdom
* Author to whom any correspondence should be addressed.
† Deceased.

E-mail: luke.harrington@waikato.ac.nz

Abstract

Southern Madagascar recently experienced a severe food security crisis, made significantly worse by well below average rainfall from July 2019 to June 2021. This exceptional drought has affected a region with high pre-existing levels of vulnerability to food insecurity (subsistence agriculture and pastoralism in the region is rain-fed only), while impacts have been compounded further by COVID-19 restrictions and pest infestations. The rainy seasons of both 2019/20 and 2020/21 saw just 60% of normal rainfall across the Grand South region and was estimated as a 1-in-135 year dry event, only surpassed in severity by the devastating drought of 1990–92. Based on a combination of observations and climate modelling, the likelihood of experiencing such poor rains in the region was not significantly increased due to human-caused climate change: while the observations and models combine to indicate a small shift toward more droughts like the 2019–2021 event as a consequence of climate change, these trends remain overwhelmed by natural variability. This result is consistent with previous research, with the Intergovernmental Panel on Climate Change (IPCC)'s Sixth Assessment Report concluding that any perceptible changes in drought will only emerge in this region if global mean temperatures exceed 2 °C above pre-industrial levels.

1. Introduction

Southern Madagascar is, at the time of writing, currently experiencing a food security crisis exacerbated by severe on-going drought. In a region where 90% of the population is living below the poverty line, recent analyses by the Integrated Food Security Phase Classification (IPC) group have concluded that tens of thousands are facing severe famine-like conditions, which have worsened with consecutive rainy season failures (2019–2021) in the otherwise semi-arid region.

In one of the hardest-hit districts of the Grand Sud (Grand South) region in Madagascar, Androy, half of all annual rainfall usually arrives during the peak months of the rainy season, from December to February, while only 20% of annual rainfall occurs during the 6 months from April to September (see figure 1). However, for two consecutive rainy seasons in 2019/20 and 2020/21, only 60% of normal rain fell across the region, causing significant crop failures in a region of largely rain-fed subsistence agriculture and pastoralism. Similar back-to-back failures of the rainy season have previously occurred in 2008–10 and 1990–92, with similar humanitarian impacts emerging then too (Benson and Clay 1998, FAO 2015). When considering 24 month rainfall accumulation periods, only the 1990–92 drought was more severe than the 2019–21 period (with ERA5 data dating back to 1950).

1.1. Event impacts

Multiple organisations, in close partnership with the government of Madagascar, have established monitoring regimes relating to the on-going risks of famine and food insecurity in the region: these organisations include the World Food Programme, The Famine Early Warning Systems Network (FEWS NET), the United Nations (via United Nations International Children's Emergency Fund (UNICEF), United Nations Population Fund (formerly United Nations Fund for Population Activities) (UNFPA), United Nations Office for the Coordination of Humanitarian Affairs (OCHA), The Food and Agriculture Organization of the United Nations (FAO) and others), and a multi-partner initiative, the IPC group.
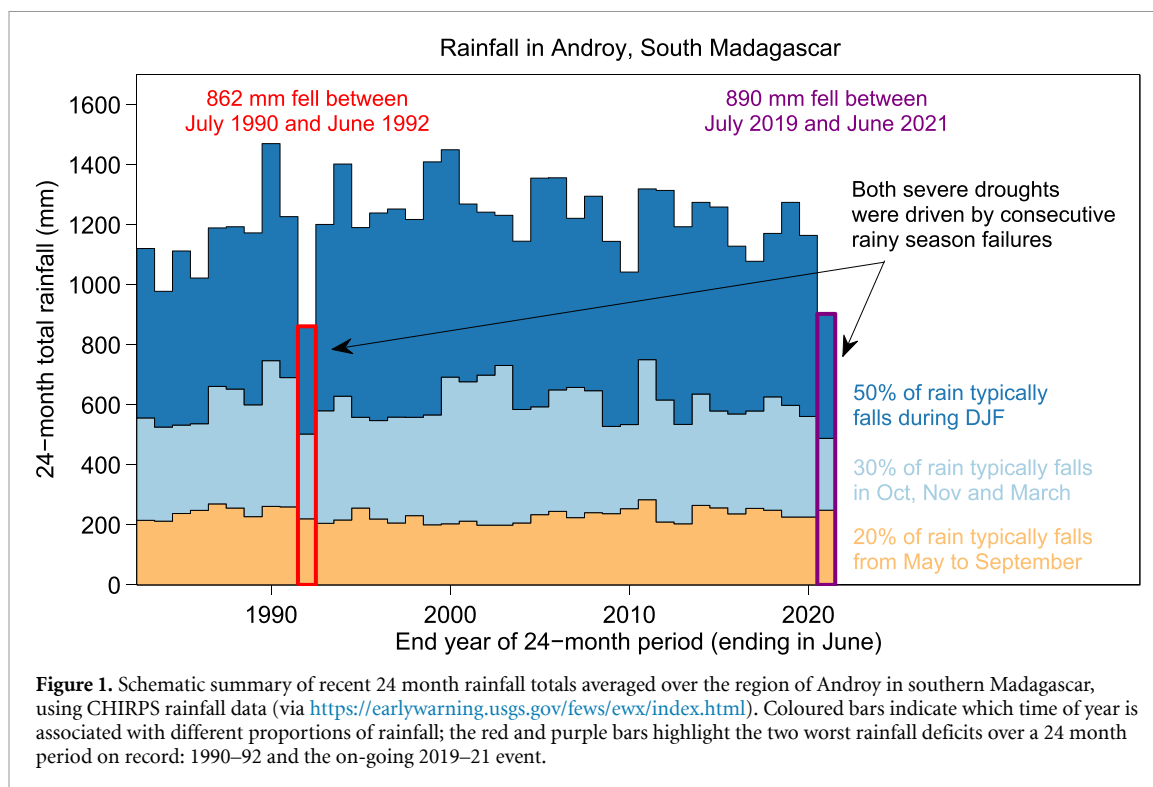
The IPC has performed in-depth analyses of on-going food insecurity challenges in the southern regions of Madagascar since 2017, using a five-tier classification system (IPC 2021). In the second half of 2019, the fraction of people in Southern Madagascar classed as needing urgent assistance (Phase 3 or above) reached a low of 14%, in part due to more reliable rainfall patterns and improved harvests allowing a slow recovery from the impacts of previous drought in 2015/16 (see figure 2). However, as both subsequent rainy seasons failed in 2019/20 and 2020/21, coupled with an array of compounding factors (see section 1.2), an April 2021 assessment by the IPC found over 43% of the population (or 1.14 million people) are facing acute food insecurity challenges (Phase 3 or above), with tens of thousands classed as Phase 5 for the first time.

1.2. Compounding factors and response measures

Food insecurity in Madagascar is not just driven by meteorological drought, but also a host of factors such as demographics, poverty, infrastructure, policy and non-climate shocks and stresses that modify the likelihood of a household becoming food insecure. Chronic food insecurity and malnutrition is particularly pervasive in Madagascar. In 2020, it was estimated that the country ranked fourth highest in the world in rates of malnutrition, with almost half of the children of 5 years or younger suffering from stunting (World Bank 2020a, World Food Programme 2021).

1.2.1. Vulnerability

Madagascar's greater southern region ('le Grand Sud') is composed of three districts: Atsimo Andrefana, Androy and Anosy. Le Grand Sud is home to approximately 2.74 million people, around 11% of the country's total population (United Nations Development Program (UNDP) 2020). It is the least developed part of the country, with a poverty incidence of 91% compared to 77% for the rest of the country (Healy *et al* 2018). Drought is considered a chronic issue in this region (Healy *et al* 2018). The people living in this region are primarily pastoralists with small scale livestock and cattle, alongside subsistence farming, growing crops like cassava, maize and sweet potatoes (FEWS NET 2020a). Water and road infrastructure in le Grand Sud is extremely poor with many roads becoming impassable during the rainy season, cutting off the region from the rest of the country (Healy *et al* 2018). Due to sparsely-distributed and poorly-maintained roads, road disruptions can easily turn into a paralysis of the whole transport network, in turn slowing down market access and ease of movement, increasing food prices and posing barriers to humanitarian response and food aid distribution. Despite roads being the backbone of intra-country trade, there has been little investment in infrastructure in the last 10 years (World Bank 2017). In Le Grand Sud, most rivers dry up for part of the year, groundwater is of poor quality and many previously dug boreholes are failing, indicating poor water availability for daily needs (Healy *et al* 2018).

Figure 1. Schematic summary of recent 24 month rainfall totals averaged over the region of Androy in southern Madagascar, using CHIRPS rainfall data (via https://earlywarning.usgs.gov/fews/ewx/index.html). Coloured bars indicate which time of year is associated with different proportions of rainfall; the red and purple bars highlight the two worst rainfall deficits over a 24 month period on record: 1990–92 and the on-going 2019–21 event.

The main rainy season in the Grand Sud is from November to March, which is a critical period for the majority of farmers that depend on rain-fed agriculture. December–March is the lean season when food tends to run out from last year's harvest, but there is not yet new food from this year's crops. When drought, locusts, storms, pests and a variety of other shocks and stresses result in lower yields, people in this region tend to sell their belongings in order to buy food (Healy *et al* 2018). In southwestern Madagascar, Zebu cattle are herded and hold strong socio-cultural value as well as being an important coping mechanism during drought years. During the 2013–2014 rainy season, one with widespread crop failure, people sold their livestock and this accounted for over 56% of cash food expenditures. However, biodiversity conservation policies, cropland expansion, and land privatization have negatively impacted pastoralism as a traditional approach to living in this semi-arid region. Security threats have also resulted in spatial and temporal shifts in grazing patterns which have a compounding impact as well leading to the risk of overgrazing and rangeland degradation (Hänke and Barkmann 2017). The second most important income source were remittances from household members who had migrated to other parts of the country for work, and many people (72% of those studied) also received food aid from non-governmental organisations (Hänke and Barkmann 2017).

1.2.2. Short-term responses
The 2019–2020 rainy season in southern Madagascar was below normal resulting in crop losses, reduced pasture and drinking water for animals (FEWS NET 2020a). In its June 2021 update, FEWS NET estimated that '2021 crop production in southern Madagascar is 10%–30% below last year and 50%–70% below the five-year average', due to a combination of sandstorms, infestations of both Fall Armyworm and migratory locusts, and low household seedstocks from 2020s high seed prices and low yields (FEWS NET 2021a).

In response to the drought and food insecurity crisis, an emergency response plan was launched by the Malagasy president at the end of August 2021 (République de Madagascar 2021). In February 2021, the Malagasy government and UN OCHA made a flash appeal for disaster response for USD 75.9 million to 1.11 million people mainly for food security, nutrition, and 'water, sanitation and hygiene' (WASH) initiatives (OCHA 2021). Government and per-government initiatives on the ground since 2021 include the building and maintenance of critical water infrastructure such as the rehabilitation of boreholes, water quality analyses, and food aid and assistance.

1.2.3. COVID-19 impacts
The COVID-19 pandemic was an important risk multiplier in the food insecurity crisis, a dynamic that has played out in a multitude of countries around the world (IFRC 2021). During March of 2020 the first COVID cases were reported in Madagascar's capital city, Antananarivo, and the government enacted measures to reduce spread, including limiting public transport and short-term lockdowns (FEWS NET 2020a).
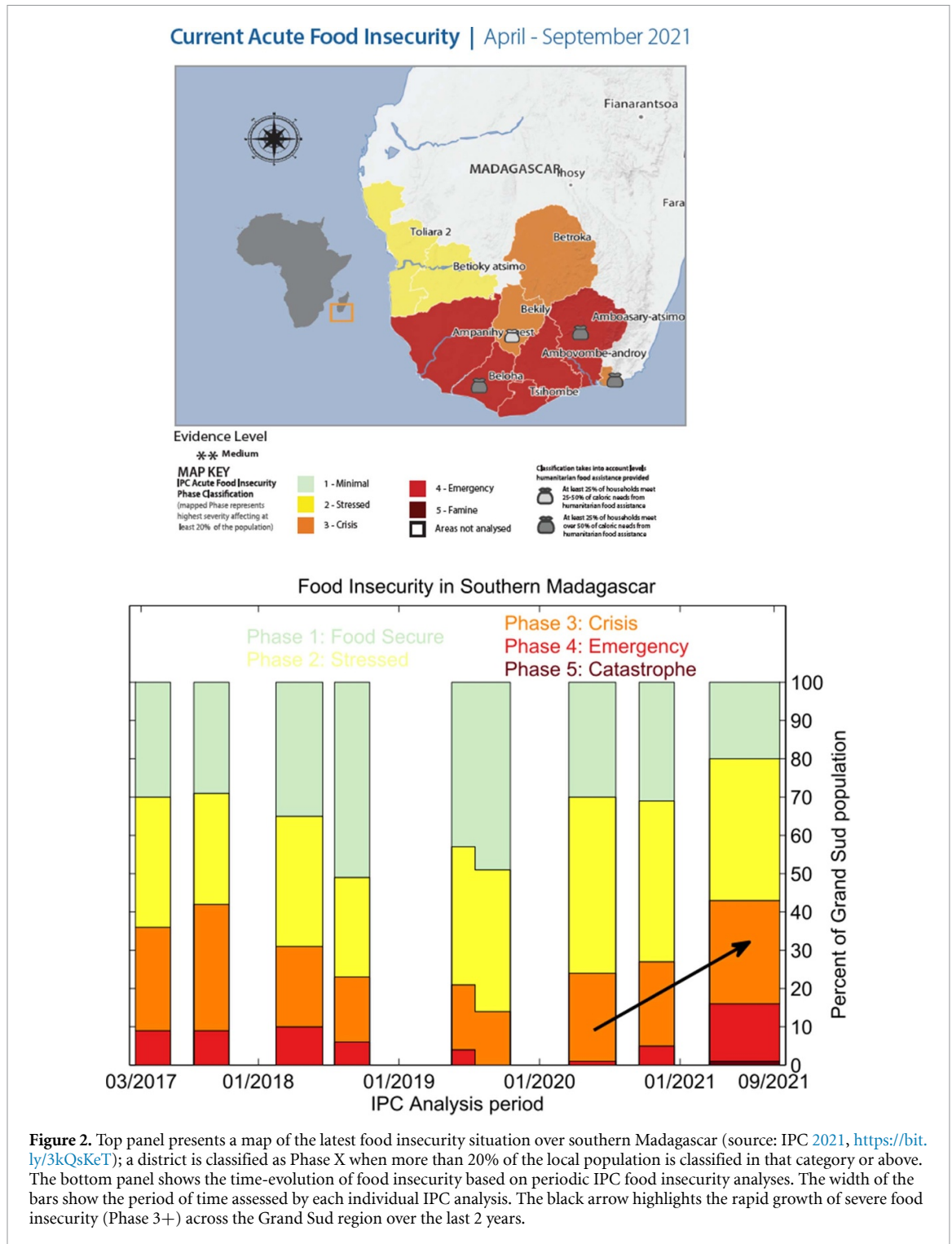
Figure 2. Top panel presents a map of the latest food insecurity situation over southern Madagascar (source: IPC 2021, https://bit. ly/3kQsKeT); a district is classified as Phase X when more than 20% of the local population is classified in that category or above. The bottom panel shows the time-evolution of food insecurity based on periodic IPC food insecurity analyses. The width of the bars show the period of time assessed by each individual IPC analysis. The black arrow highlights the rapid growth of severe food insecurity (Phase 3+) across the Grand Sud region over the last 2 years.

Overall, the stay-at-home orders and other measures, necessary to limit the spread of COVID-19 and prevent health infrastructure from being overwhelmed, negatively impacted people's ability to migrate for casual labour—a key source of income for communities in Southern Madagascar as well as a way to modulate the negative impacts of a poor yield year (FEWS NET 2020b, 2021a). The COVID-19 measures disrupted supply chains around the world and within Madagascar, exacerbating price hikes for staple foods and limiting access to markets (FEWS NET 2020b). The tourism, mining and textile industries were also disrupted by COVID-19, which in turn reduced the number of jobs available for those who were able to migrate once restrictions were lifted, thereby having a dampening effect on the local economy (FEWS NET 2020f, 2021b). This lack of alternative income sources led to more people relying on farming to make a living, further exacerbating the impact of the drought on local livelihoods.

2. Defining the drought 'event'

Droughts are comparably complex extreme events which depend on a number of climate and non-climate factors, as well as their interactions. Examples of the former include precipitation, temperature and soil- and vegetation-related feedbacks; examples of the latter include agricultural practices, the use of irrigation and choices around grazing density (van Loon *et al* 2016). Accordingly, there are several definitions of drought in use, with meteorological drought (precipitation deficit), hydrological drought (low streamflow), agricultural and ecological drought (low soil moisture combined with high evaporative demand) being the most common (Seneviratne *et al* 2021).

This complexity of drought poses challenges for their attribution, and in particular selecting the most appropriate event definition. With increasing temperatures, there is an *a priori* assumption that droughts are also becoming more severe. However, the link between droughts and climate change is often more complex: while agricultural and ecological droughts have increased in drought-prone areas like Southern Africa and the Mediterranean region, this is not the case for other types of drought nor for other arid regions, like Eastern Africa (Seneviratne *et al* 2021). For Madagascar as a whole, chapters 11 and 12 of the Intergovernmental Panel on Climate Change (IPCC)'s Sixth Assessment Report (Ranasinghe *et al* 2021, Seneviratne *et al* 2021) determined with *medium confidence* that both meteorological and agro-ecological droughts will increase in response to global mean warming in excess of ∼2 °C, but a more regional assessment specifically for the Grand Sud has not been performed.

Importantly, Kew *et al* (2021) systematically examined different methods of defining drought in the context of extreme event attribution for a sequence of both arid and semi-arid regions in East Africa, including those with a climate comparable to that of south-west Madagascar (Beck *et al* 2018; see appendix 1 for supporting details). The authors used a range of observational products, regional climate models (RCMs), hydrological models and other impact models to explicitly decompose attributable changes in temperature, precipitation, evaporative demand and soil moisture associated with drought in a changing climate. Their results found that, while all analysed sub-regions did exhibit robust and statistically significant increases in temperature, this did not translate to corresponding increases in the likelihood of witnessing exceptional soil moisture deficits. Instead, they found that drought in these regions was primarily driven by precipitation deficits, while anomalously high temperatures did not necessarily exacerbate corresponding soil moisture anomalies. Such a result is supported by Manning *et al* (2018), who found that the influence of precipitation on subsequent soil moisture deficits was much larger than that of temperature (via changes in evaporative demand) in water-limited observational settings.
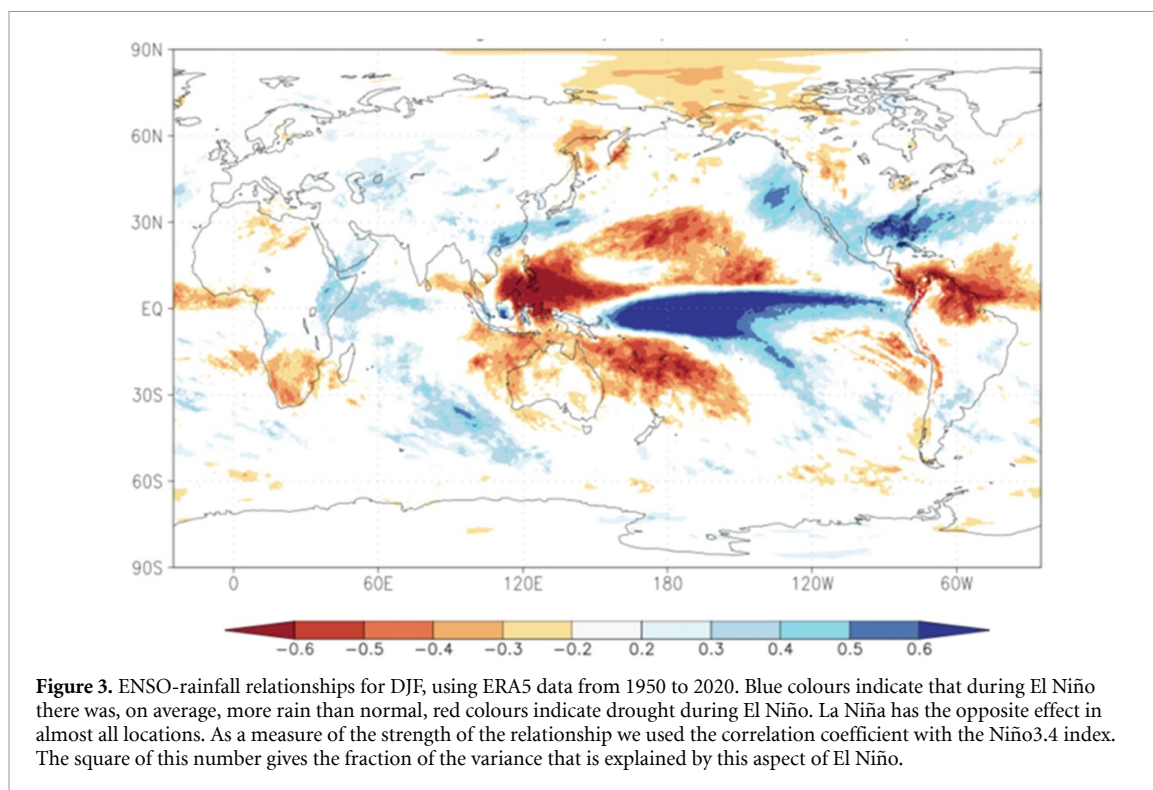
Given these findings, the limited reliability of observations other than rainfall and temperature in this region, and the fact that precipitation deficits (i.e. meteorological drought) are used as a key determinant in regional drought forecasts and early warning systems, we focus on rainfall deficits in this analysis. Nevertheless, it is acknowledged that anomalously high temperatures in the area have almost certainly increased in frequency and intensity due to anthropogenic climate change: future studies employing appropriate modelling tools (including coupled hydrological models) to examine soil moisture changes directly over this region would therefore be useful to resolve the relationship between drought and temperature further.

2.1. Climatological context

The climate of Madagascar varies from humid tropical in the east to semi-humid tropical over the central and western parts of the country, while the south is mainly semi-arid. The island is therefore characterized by strong east–west and north–south rainfall gradients. This spatial heterogeneity arises due to the complex interaction of different climate drivers across multiple scales, spanning from small-scale mesoscale processes to synoptic-scale teleconnections. The north–south mountain chain, reaching over 2600 m in places and running along the eastern part of the island, interacts with moist air masses brought by the trade winds from the western Indian Ocean, leading to orographically enhanced rainfall year-round along the east coast. The mountains, on the other hand, act as a rain shadow for the western areas. The amount of rain in the east is therefore 2–3 times larger than that of the west (Jury *et al* 1995).

Rainfall peaks during the austral summertime, enhanced by deep convection associated with tropical convergence: the southernmost position of Intertropical Convergence Zone establishes itself over the central part of the island (17–20° S) at the peak of the austral summer (Jury *et al* 1995, Randriamahefasoa and Reason 2017).

The north-western part of the island receives summer rainfall primarily through NE monsoon winds originating from the western tropical Indian Ocean and recurving over the northern Mozambique Channel to become rain-bearing north-westerlies. The area is also characterized by rainfall from the strong mesoscale convective systems occurring in the northern Mozambique Channel. In addition, rainfall in the northern

Figure 3. ENSO-rainfall relationships for DJF, using ERA5 data from 1950 to 2020. Blue colours indicate that during El Niño there was, on average, more rain than normal, red colours indicate drought during El Niño. La Niña has the opposite effect in almost all locations. As a measure of the strength of the relationship we used the correlation coefficient with the Niño3.4 index. The square of this number gives the fraction of the variance that is explained by this aspect of El Niño.

part of the island is also associated with low geopotential height over the southwestern Indian Ocean (Fauchereau *et al* 2009, Jury 2016). In contrast, rainfall in the southern region tends to be modulated by the Mozambique Channel Trough (Barimalala *et al* 2018) and heavily influenced by less saturated air masses originating over the south-western Indian Ocean, with the south-west remaining mostly leeward and therefore relatively dry. Rainfall in the southern region is also driven by tropical temperate troughs—large convective systems linking the easterly subtropical wave to mid-latitude westerlies' frontal systems (Hart *et al* 2013, Macron *et al* 2016)—as well as cut-off lows (Favre *et al* 2013, Hart *et al* 2013).

Madagascar is also frequently affected by tropical cyclones (TCs) forming in the south-west Indian Ocean, although they mostly impact the East Coast of Madagascar. The south-west of the island is rarely impacted, although TC Favio in 2007 tracked close to the south and southwestern coasts (Klinman and Reason 2008) and TC Dera in 2001 tracked southwards through the Mozambique Channel and passed close to the south-western coast of Madagascar (Reason 2007). In late January 2019, tropical storm Eketsang tracked along the south-western coast of Madagascar, delivering double the rainfall expected for that month across the region.

2.2. Influence of modes of natural variability

Wet-season precipitation is highly variable over southern Madagascar (see top-right panel of figure 7). Several modes of natural climate variability are known to modulate seasonal rainfall over the wider Southern Africa region, including the El Niño Southern Oscillation (ENSO), the Indian Ocean Dipole (IOD) and the sub-tropical IOD (sIOD) (Hoell *et al* 2015, 2017, Hart *et al* 2018). However, the extent to which these modes of variability represent a causal driver of the recent rainfall deficits over southern Madagascar remains less clear.

Generally speaking, the majority of impacts driven by significant IOD 'events' occur well to the north of Madagascar—they can be significant over the Horn of Africa, for example (Cai *et al* 2021; figure 1(b) from, Abram *et al* 2020). While the months of October to November 2019 did mark the peak of a severe positive IOD event, rainfall was mostly average over southern Madagascar until later in December that year. Moreover, there were also significant IOD events in 1994, 1997 and 2006 (Cai *et al* 2021), none of which aligned with significant drought events over southern Madagascar (figure 1).

When examining the relationship between NINO3.4 index and December–February (DJF) rainfall globally (using ERA5), a statistically significant relationship between ENSO and seasonal rainfall was found over both Southern Africa and Eastern Africa, with El Niño events aligning with low- and high-rainfall anomalies, respectively (figure 3). However, the strength of this correlation was less significant over southern Madagascar, with similarly weak results also found when looking instead over the months of September to November or when considering Global Precipitation Climatology Centre (GPCC) rainfall data (not shown).

Figure 4. Average annual rainfall (in units of mm d^{-1}) over 1951–2020, using data from ERA5.
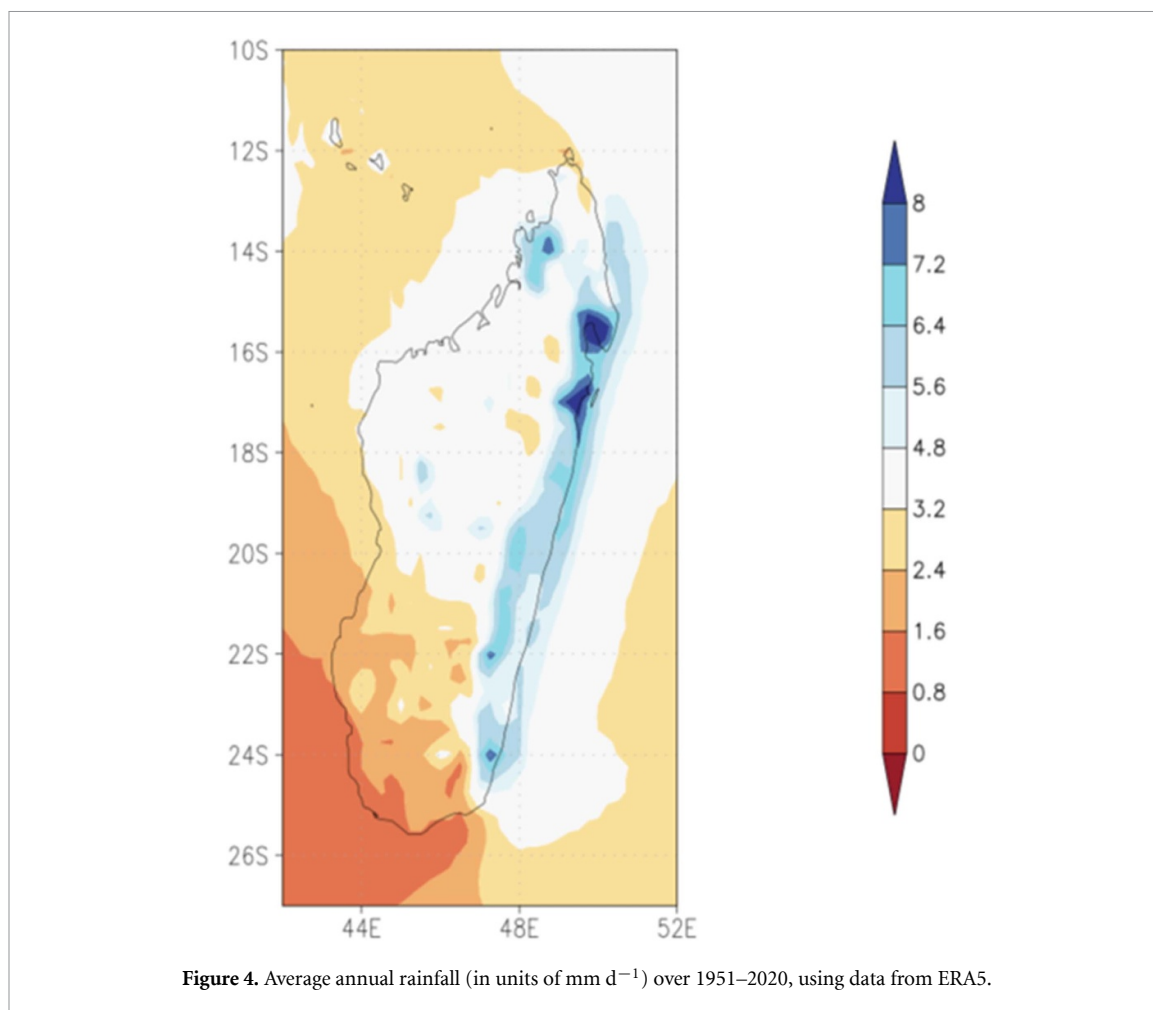
Past instances of back-to-back precipitation deficits during the rainy season (1990–92) have coincided with moderate-strong El Niño events, as did the dry summer of 2015/16. Hoell *et al* (2017) suggests, for example, that an El Niño event aligning with an opposite-signed sIOD phase offers good predictability of low rainfall over the region in question. However, such criteria were indeed met during the severe El Niño of 1997/98 and yet coincided with a normal rainy season over southern Madagascar. Moreover, the back-to-back poor rainy seasons in 2008–10 alternated between positive and negative ENSO phases, while the extremely dry summer of 2020/21 coincided with a moderate-strength La Niña event (the summer of 2019/20 was ENSO-neutral).

Altogether, external modes of variability appear to have played little if any role in the formation of the event.

2.3. Spatial and temporal characteristics

To determine the best choice of spatial domain for the attribution analysis requires a balance of multiple considerations, including where the impacts are most pronounced (section 1.1), differences in climate and land characteristics between different sub-regions of Madagascar (figure 4), as well as the meteorological features of the drought itself.

Looking first at the magnitude of rainfall deficits across the country using two different observation-related rainfall products Climate Hazards Group InfraRed Precipitation with Station (CHIRPS and ERA5; see section 3.1 for further details), figure 5 confirms the southern regions of the country that have borne the worst humanitarian impacts of the drought are also those regions where annual rainfall deficits have been particularly severe for each of the last 2 years. Considering all lines of evidence together, and with a particular weight placed on the concentrated humanitarian impacts in the very south of the country, we chose to hereafter define the spatial bounds of the drought event using latitude bounds of 23.5°S to 25.5°S and longitude bounds of 43.5°E to 47°E—this region is represented by the purple rectangles in figure 5, and is also referred to as the 'Grand Sud' region in the remainder of the analysis.

Figure 6 shows the time-evolution of recently observed rainfall anomalies when averaging across this region of interest (where red and blue shading respectively indicates a drier-than-average and
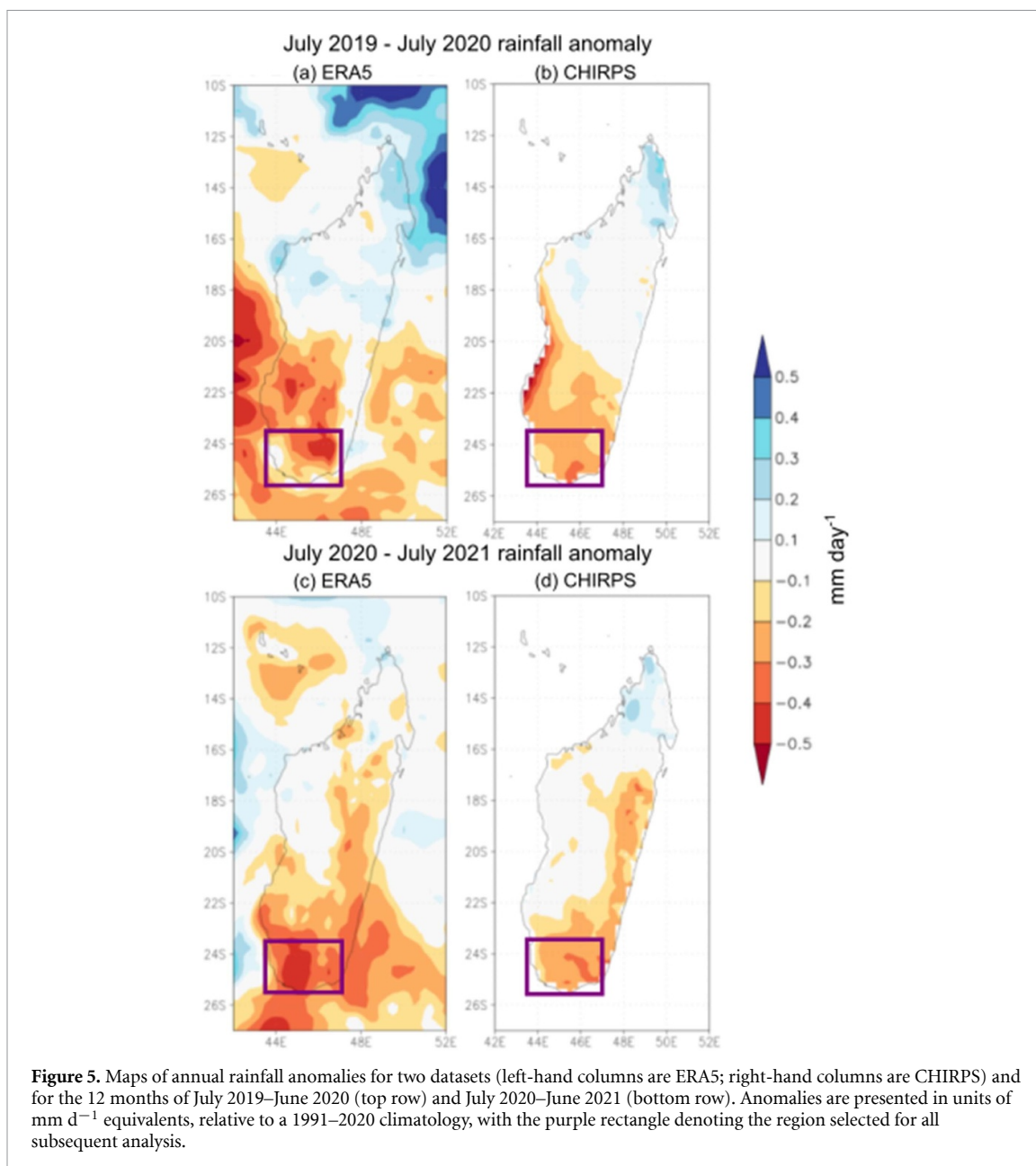
Figure 5. Maps of annual rainfall anomalies for two datasets (left-hand columns are ERA5; right-hand columns are CHIRPS) and for the 12 months of July 2019–June 2020 (top row) and July 2020–June 2021 (bottom row). Anomalies are presented in units of mm d^{-1} equivalents, relative to a 1991–2020 climatology, with the purple rectangle denoting the region selected for all subsequent analysis.

wetter-than-average month). There exists robust agreement across datasets of the following features: (a) the lack of rainfall during the last two wet seasons (and particularly the 14 months spanning December 2019 to January 2021) has been particularly severe; (b) while January of 2019 represented an extremely wet month in the region, rainfall was also average throughout the entire 2018/19 hydrological year; and (c) the magnitude of any rainfall deficits during the rainy seasons of 2016/17 and 2017/18 were not considered significant, and likely counteracted by wetter-than-average shoulder seasons. For these reasons, coupled with the corresponding Standardised Precipitation Index (SPI) calculations shown in panel (c), we have chosen to define the length of the drought event as total rainfall for the 24 month period spanning July 2019–June 2021 (inclusive).

2.4. Previous research

To our knowledge, there have been no attribution studies examining individual weather events over Madagascar. The IPCC Sixth Assessment Report classified the region as exhibiting 'low confidence' of observed human influence on drought, 'due to limited evidence'. For those studies which have instead examined future projections of rainfall over the region, most generally conclude that annual mean rainfall is projected to decrease under moderate- and high-emissions climate scenarios, but this signal of change has yet to emerge from the 'noise' of internal variability in the current climate.
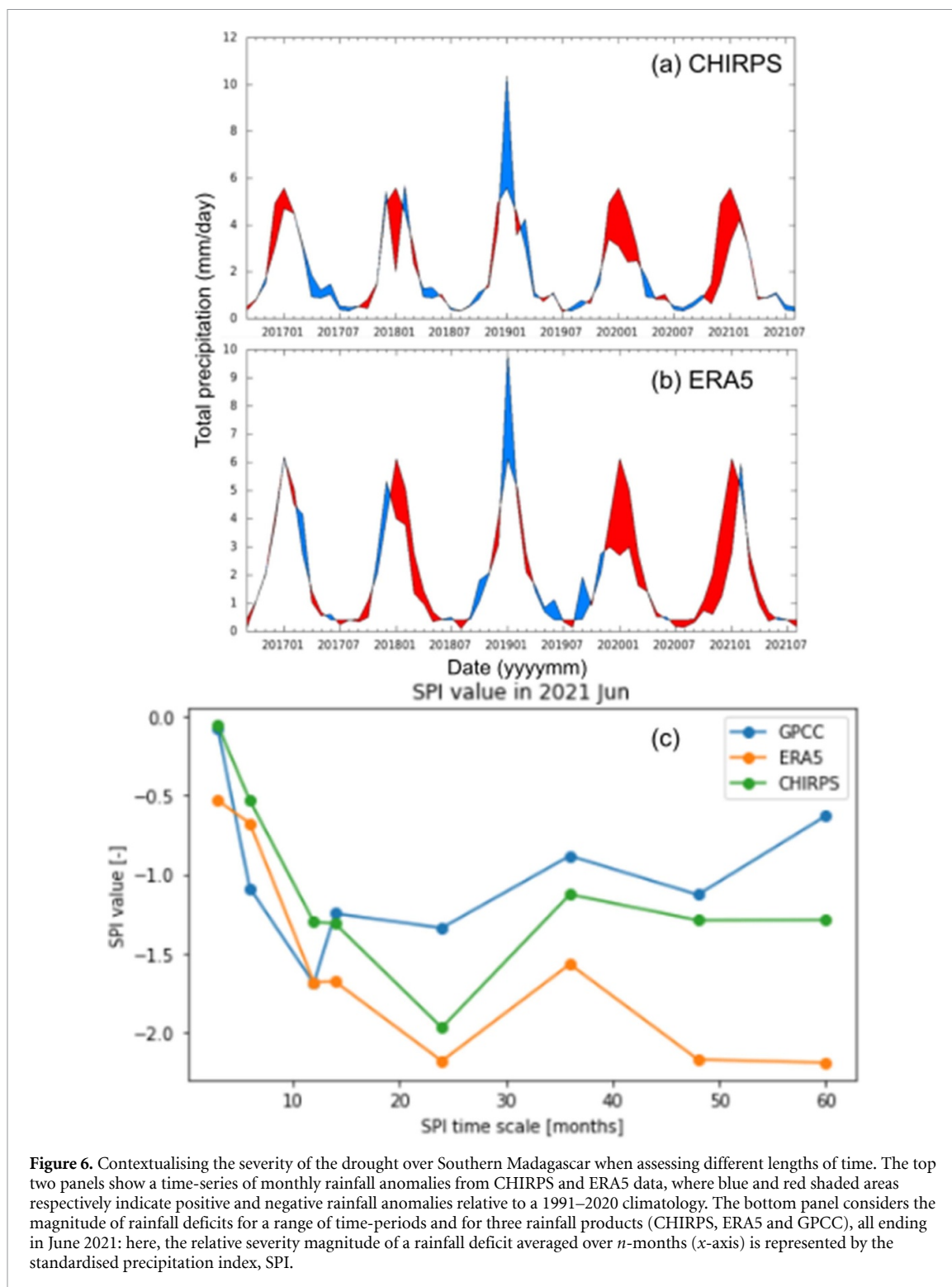
Figure 6. Contextualising the severity of the drought over Southern Madagascar when assessing different lengths of time. The top two panels show a time-series of monthly rainfall anomalies from CHIRPS and ERA5 data, where blue and red shaded areas respectively indicate positive and negative rainfall anomalies relative to a 1991–2020 climatology. The bottom panel considers the magnitude of rainfall deficits for a range of time-periods and for three rainfall products (CHIRPS, ERA5 and GPCC), all ending in June 2021: here, the relative severity magnitude of a rainfall deficit averaged over *n*-months (*x*-axis) is represented by the standardised precipitation index, SPI.

2.4.1. Historical trends

Randriamarolaza *et al* (2021) examined observed trends from 28 weather stations across the country, and found observed decreases in rainfall in some stations across Madagascar and corresponding increases in drought-related indices. However, trends were largely statistically insignificant and no station data were available over the Grand Sud region most affected by the on-going food security crises. Our analysis of data from the nearest available weather stations in GHCN-D (see appendix 2) found large data gaps which prevented any complementary analysis of observed rainfall trends.

Lim Kam Sian *et al* (2021) found no statistically significant trends in observed rainfall from 1900 to 2014, when considering the months of May to October and November to April individually for both observation-derived rainfall datasets (GPCC, Climatic Research Unit (CRU) and UDel) and corresponding Coupled Model Intercomparison Project Phase 6 (CMIP6) model simulations.

Synthesizing the evidence of rainfall and drought trends for Madagascar as a whole, including assessments relating to dry-season water availability by Padrón *et al* (2020), Seneviratne *et al* (2021) concluded there were no consistent trends of observed changes in drought over the region.

2.4.2. Future projections

Lim Kam Sian *et al* (2021) examined 21st century projections of seasonal rainfall change in CMIP6 models under medium- and high-warming scenarios (SSP2-4.5 and SSP5-8.5). While any projected changes in wet-season (December–March (DJFM)) rainfall were statistically insignificant, trends of decreasing May–October rainfall were found to emerge across Madagascar in the second half of the 21st century under an SSP5-8.5 scenario, with drying signals more evident over the east of the country.

Coppola *et al* (2021) examined future changes in the frequency of meteorological drought events over Madagascar for a range of different climate model experiments and scenarios, including high- and low-emission scenarios from Coupled Model Intercomparison Project Phase 5 (CMIP5), CMIP6 and multiple coordinated regional climate downscaling experiment (CORDEX) regional model experiments. The authors focused on the SPI for a time window of 6 months (SPI-6) and chose to define a drought as starting in any month when SPI-6 falls below 1, and ending when SPI-6 returned to positive values for at least two corresponding months. When defined in this manner, Coppola and colleagues found most models to overestimate observed drought frequency (identifying 2–3 events per decade instead of the observed 1–2), while best-guess estimates across all model ensembles projected an additional one to two droughts per decade by mid-century. Using the same index, the IPCC (2021, ch 12, figure 4) found a consistent increase in the number of drought events across model ensembles (CMIP5, CMIP6 and CORDEX) by late-century under representative concentration pathway 8.5 (RCP8.5) or SSP5-8.5.

Barimalala *et al* (2021) presented a comprehensive analysis of projected climate changes under 1.5° and 2° of warming specifically for Madagascar, using RCMs from the CORDEX-Africa ensemble. Robust decreases in rainfall were projected for northern and eastern parts of the country during the months of October to December at these thresholds of future warming, while statistically insignificant changes were projected for the southern and western regions of the country currently experiencing on-going drought impacts. This spatial heterogeneity is in agreement with Lim Kam Sian *et al* (2021), offering important context when interpreting country-level syntheses seen elsewhere, like the Interactive Atlas of the IPCC Sixth Assessment Report (https://interactive-atlas.ipcc.ch/regional-information). The authors also report mostly non-significant increases in rainfall during the wetter months of January to April across the country, with more pronounced increases again in the north and east of the country.

Dosio *et al* (2019) also performed an in-depth assessment of the significance and robustness of future changes in both mean rainfall as well as extreme precipitation-related indices over the country, albeit analysing end-of-century (2081–2100) simulations from CORDEX-Africa under a high-warming RCP8.5 scenario. They confirmed the results of previous work, showing that high levels of global warming lead to robust projected reductions in season mean rainfall over September–November (SON) (particularly eastern and northern regions) and smaller but statistically significant increases in rainfall during DJF. Robust increases in both the intensity of extreme wet days and in the frequency of consecutive dry days were also reported, with these extreme indices showing larger signals of change than in the mean.
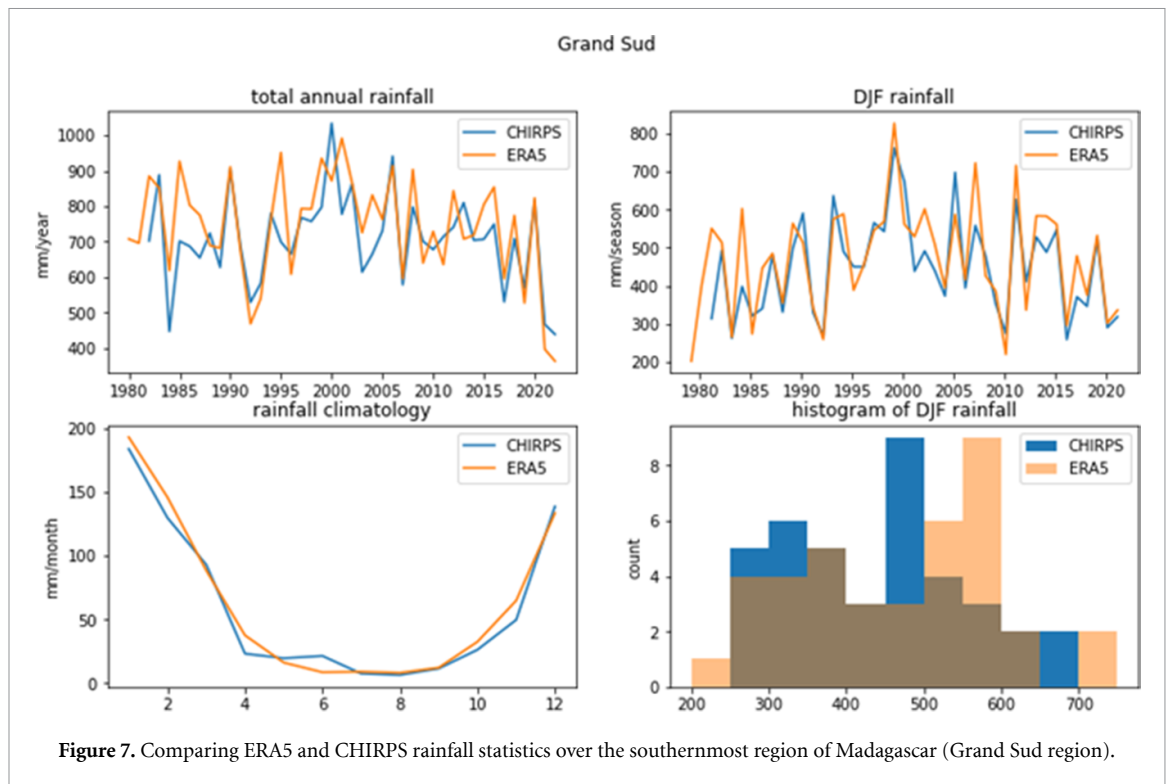
Finally, Kendon *et al* (2019) examined end-of-century (under RCP8.5) changes in wet-season rainfall characteristics over the African continent, using a 4.5 km resolution convection-permitting climate model. Results show evidence of statistically significant increases in wet-season mean rainfall over southwestern Madagascar in a high-warming scenario, with changes being largely driven by corresponding increases in the intensity of the most extreme rainfall events.

Combined, previous research suggests that future warming over the 21st century could lead to small-to-moderate increases in wet-season rainfall over southern Madagascar (largely driven by the intensification of the wettest days of the year), while the latter half of the dry season (August–October) is projected to become drier and longer. The sign of change is mostly consistent across Madagascar, although the magnitude of these relative changes are more pronounced in northern and eastern regions. Most modelling studies further suggest that such changes—as well as corresponding signals of change in average rainfall over one or two consecutive years—are unlikely to be statistically significant (or have 'emerged' from the 'noise' of internal variability) after only 1.2 °C of global temperature rise.

3. Data and methods

3.1. Observational data

Several options exist when evaluating a recent extreme weather event in the context of historical climate observations. While analysing historical data from local weather stations is the first preference for any study,

Figure 7. Comparing ERA5 and CHIRPS rainfall statistics over the southernmost region of Madagascar (Grand Sud region).

we found no station data of sufficient quality within the region of interest, having evaluated available station data within the Trans-African Hydro-Meteorological Observatory (TAHMO), Global Historical Climatology Network (GHCN) and CRU datasets (see appendix 2 for further details).

Rainfall data from 'Climate Hazards Group InfraRed Precipitation with Station data' (CHIRPS; Funk *et al* 2015) is frequently used for analyses over the Southern Africa region (including by FEWS NET for their food insecurity projections) and was thus considered for our analysis. However, due to the relatively short length of the CHIRPS dataset (dating back to 1981) we restrict our use of the CHIRPS dataset to only examining the characteristics of the event and comparing with other datasets: the length of the CHIRPS dataset does not, for example, allow us to successfully fit a generalised Pareto distribution (GPD) with only the lowest 20% of data (see section 3.3 for an explanation).

Because we were interested in analysing time-series which are as long as possible, we have also examined precipitation data from the European Centre for Medium-Range Weather Forecasts via their ERA5 reanalysis product (which dates back to 1950; Hersbach *et al* 2020). Figure 7 presents statistical characteristics of the two datasets over the Grand Sud region of Madagascar, revealing good agreement on both seasonal rainfall characteristics as well as on the timing of previous drought events.

As a measure of anthropogenic climate change, we use the (low-pass filtered) global mean surface temperature (GMST), where GMST is taken from the National Aeronautics and Space Administration Goddard Institute for Space Science surface temperature analysis (Hansen *et al* 2010, Lenssen *et al* 2019).

3.2. Model and experiment descriptions
For the attribution of the drought event, three different model ensembles are used.

The first is the CORDEX-Africa (0.44° resolution, AFR-44) multi-model ensemble (Nikulin *et al* 2012). The ensemble used consists of 22 simulations resulting from pairings (as of November 2021) of global climate models (GCMs) and RCMs (see table 1 below). These simulations are composed of historical simulations up to 2005 and then extended to the end of the 21st century using the RCP8.5 scenario. For each simulation, we consider the entire period available for attribution. All models were tested for the GPD parameters against observations and one model was removed because the 95% confidence intervals were not overlapping with the ERA5 confidence intervals.

The second ensemble is the HighResMIP SST-forced model ensemble (Haarsma *et al* 2016), spanning 1950–2050. For the 'present' time period (1950–2014), the SST and sea ice forcings used in the HighResMIP are based on the daily, 0.25° × 0.25° Hadley Centre Global Sea Ice and Sea Surface Temperature dataset, with area-weighted regridding used to map this to each model grid. For the 'future' time period (2015–2050), SST/sea-ice data are derived from RCP8.5 (CMIP5) data, and combined with greenhouse gas forcings from

Table 1. List of the RCMs used with their driving GCMs and the period simulated (see Nikulin *et al* (2012) for a description of the RCMs and Taylor *et al* (2012) for the GCMs). The RCA4 downscaling MIROC5 was removed after model evaluation.

RCM	GCM	Years
RCA4	CanESM2	1951–2099
	EC-EARTH	1951–2099
	CNRM-CM5	1951–2099
	HadGEM2-ES	1951–2099
	MPI-ESM-LR	1951–2099
	IPSL-CM5A-LR	1951–2099
	CSIRO-Mk3-6-0	1951–2099
	NorESM1-M	1951–2099
	MIROC5	1951–2099
	GFDL-ESM2M	1951–2099
	CNRM-CM5	1950–2099
CCLM4-8-17	HadGEM2-ES	1949–2097
	EC-EARTH	1949–2098
	MPI-ESM-LR	1949–2098
HIRHAM5	EC-EARTH	1951–2099
RACMO22T	EC-EARTH	1950–2099
	HadGEM2-ES	1950–2098
	EC-EARTH	1950–2099
	HadGEM2-ES	1950–2098
REMO2009	MPI-ESM-LR	1950–2099
	IPSL-CM5A-LR	1950–2099
	MIROC5	1950–2099

Table 2. List of five climate models analysed from the HiResMIP SST-forced experiment, including their spatial resolution.

HiResMIP model	Institution	Horizontal resolution
CNRM-CM6-1-HR	Centre National de Recherches Meteorologiques	∼50 km
EC-Earth3P-HR	EC-Earth-Consortium	∼40 km
HadGEM3-GC31-HM	Met Office Hadley Centre	∼25 km
CMCC-CM2-VHR4	Fondazione Centro Euro-Mediterraneo sui Cambiamenti Climatici	∼25 km
MPI-ESM1-2-XR	Max Planck Institute for Meteorology	∼60 km

SSP5-8.5 (CMIP6) simulations (see section 3.3 of Haarsma *et al* 2016 for further details). For each simulation, we consider the time period up to the event (1950–2021) for attribution. We also tested using the entire time period (1950–2050) to increase the sample size, though this sensitivity test yielded negligible differences in the final results (not shown).
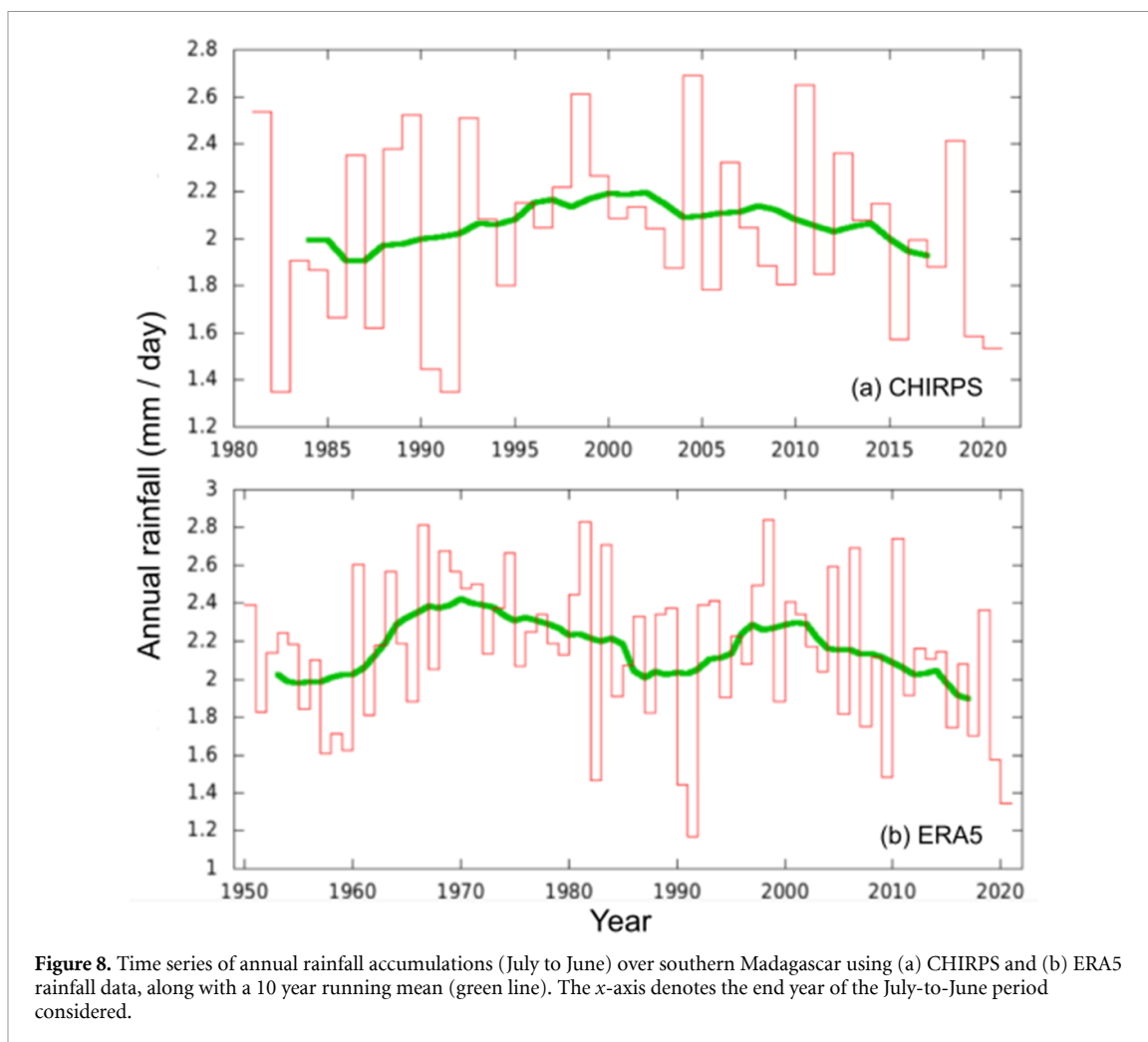
For HighResMIP, only those models with a spatial resolution comparable with ERA5 and CHIRPS are considered in this analysis, with one ensemble member used from each model (table 2).

We also use five ensemble members of simulations from both the AM2.5C360 (Yang *et al* 2021, Chan *et al* 2021) and forecast-oriented low ocean resolution (FLOR) (Vecchi *et al* 2014) climate models developed at Geophysical Fluid Dynamics Laboratory (GFDL). AM2.5C360 is an atmospheric GCM with a horizontal resolution of 25 km. Its five ensemble simulations are Atmospheric Model Intercomparison Project (AMIP) experiment (1871–2021) initialized from five different pre-industrial conditions but forced by the same SSTs from HadISST1 (Rayner *et al* 2003) after groupwise adjustments (Chan *et al* 2021), as well as the same historical radiative forcings. The FLOR model, on the other hand, is an atmosphere-ocean coupled GCM with a resolution of 50 km for land and atmosphere and 1° for ocean and ice. The five ensemble simulations cover the period from 1860 to 2100 and include both the historical and RCP4.5 experiments driven by transient radiative forcings from CMIP5 (Taylor *et al* 2012).

3.3. Statistical methods
In this analysis we examine 24 month running mean rainfall data (from July to June), averaged over the southern Madagascar region (as defined in section 1.2). Methods for observational and model analysis and for model evaluation and synthesis are used according to the World Weather Attribution Protocol, described in Philip *et al* (2020), with supporting details found in van Oldenborgh *et al* (2021) and Ciavarella *et al* (2021).

The analysis steps include: (a) trend calculation from observations; (b) model evaluation; (c) multi-method multi-model attribution and (d) synthesis of the attribution statement.

Figure 8. Time series of annual rainfall accumulations (July to June) over southern Madagascar using (a) CHIRPS and (b) ERA5 rainfall data, along with a 10 year running mean (green line). The *x*-axis denotes the end year of the July-to-June period considered.

We calculate the return periods, probability ratio (PR) and change in intensity of the event in question when comparing observed GMST values of 2021 with past GMST values (1850–1900, based on the Global Warming Index www.globalwarmingindex.org), an estimated difference of 1.2 °C.

To statistically model the event in question, we adopt the approach of Kew *et al* (2021) and references therein, using a GPD that scales with GMST, and fitted to the lowest 20% of the data to focus on low precipitation extremes. When scaling with GMST as a covariate, the location and scale parameters are both adjusted, such that the ratio of the two (i.e. the dispersion parameter) remains unchanged. To account for the autocorrelation associated with the 2 year running mean, the error margins associated with the GPD fit were computed with a moving block bootstrap with a block size of 2 years.
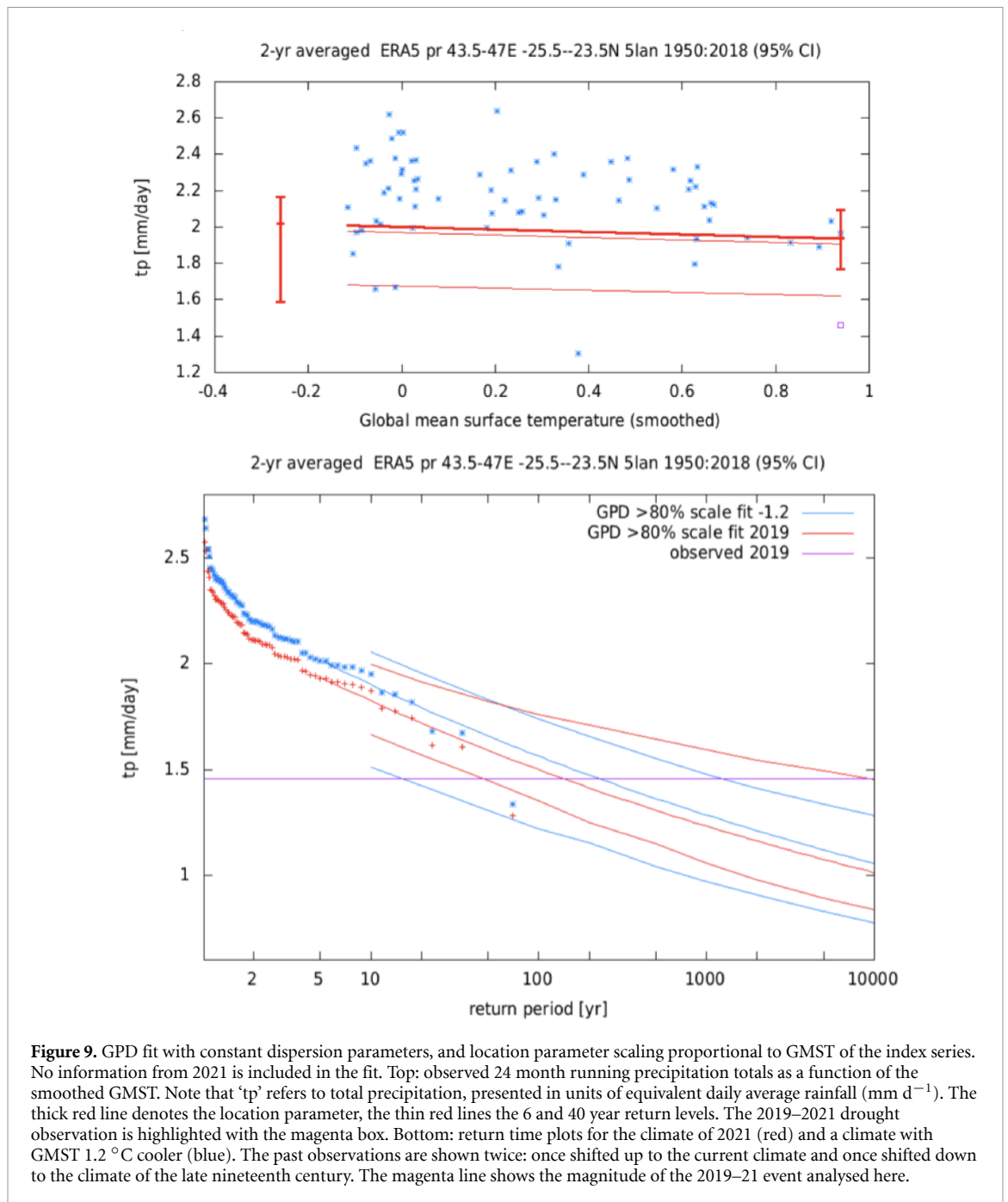
Finally, results from observations and models that pass the validation tests (see section 4) are synthesized into a single attribution statement.

4. Observational analysis: return time and trend

4.1. Analysis of gridded data
Figure 8 shows a time-series of annual rainfall for the two observational datasets considered. As explained in section 2.1, we only examine warming-related trends in rolling 24 month rainfall accumulations with the ERA5 data, as the length of the CHIRPS data is too short to meet the statistical requirements for a GPD-based analysis.

Figure 9 presents the trend fitting methods applied to the ERA5 transient series and time slices, respectively. In the top panel, the thick red line denotes the location parameter scaled with GMST, while the thin red lines denote the corresponding 6 and 40 year return levels of low-rainfall anomalies. The bottom panel presents return time plots for the climate of 2021 (red) and a climate with GMST 1.2 °C cooler. The magenta horizontal line indicates the average daily mean rainfall observed across the 24 months of the 2019–21 drought: rainfall deficits of this magnitude correspond to a best-guess return period of

Figure 9. GPD fit with constant dispersion parameters, and location parameter scaling proportional to GMST of the index series. No information from 2021 is included in the fit. Top: observed 24 month running precipitation totals as a function of the smoothed GMST. Note that 'tp' refers to total precipitation, presented in units of equivalent daily average rainfall (mm d^{-1}). The thick red line denotes the location parameter, the thin red lines the 6 and 40 year return levels. The 2019–2021 drought observation is highlighted with the magenta box. Bottom: return time plots for the climate of 2021 (red) and a climate with GMST 1.2 °C cooler (blue). The past observations are shown twice: once shifted up to the current climate and once shifted down to the climate of the late nineteenth century. The magenta line shows the magnitude of the 2019–21 event analysed here.

1-in-135 years in today's climate (the intersection of the middle red line), albeit with high levels of uncertainty (the outer red lines).
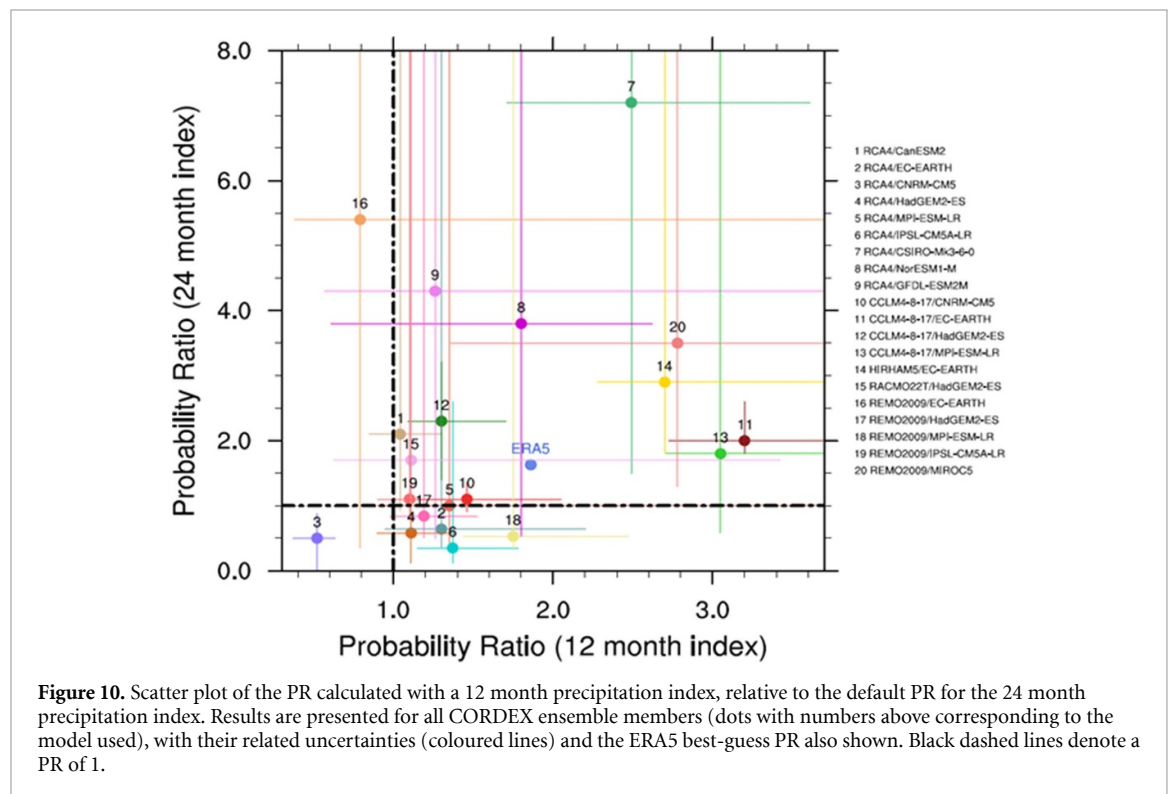
5. Multi-method multi-model attribution

Here, we calculate the probability ratio (PR), as well as the change in magnitude of the event, in both the observations and the models. For each model considered, we focus on the change in frequency and intensity associated with a 1-in-135 year event (which was the best estimate of the observed event's rarity) as defined within that model. Only models which passed a sequence of validation tests (detailed further in the supplementary information) are presented below.

Table 3 shows the PRs and change in intensity for ERA5, CHIRPS and for the models that passed our validation tests (see table S1). Note again that values for CHIRPS in table 3 are calculated using the lowest 30% of precipitation in the GPD fit rather than the lowest 20% and therefore cannot directly be compared to the other values. In the synthesis (section 6), we therefore only include ERA5 and not CHIRPS.

Table 3. Analysis results showing the model threshold for a 1-in-135 year event in the current climate, and the PRs and intensity changes for the present climate with respect to a pre-industrial climate which is 1.2 °C cooler than today. Note that the values listed for ERA5 and CHIRPS in the second column refer to the observed event magnitudes.

Model/observations	Threshold for return period 135 year	Probability ratio PR (-)	Change in intensity ΔI (%)
ERA5	**1.46 mm d^{-1}**	**1.6 (0.0064 .. 5.4)**	**−4.1 (−14 … 30)**
CHIRPS lowest 30%. Not used for validation.	**1.56 mm d^{-1}**	**6.1 (0.021 … 30)**	**−13 (−22 … 38)**
RCA4/CanESM2	0.90 mm d^{-1}	2.1 (0.93 … ∞)	−4.2 (−15 … 0.46)
RCA4/EC-EARTH	1.7 mm d^{-1}	0.64 (0.37 … 17)	1.8 (−5.7 … 4.2)
RCA4/CNRM-CM5	2.4 mm d^{-1}	0.50 (0.019 … 0.88)	3.4 (0.59 … 7.1)
RCA4/HadGEM2-ES	1.8 mm d^{-1}	0.58 (0.12 … 9.2)	1.3 (−3.4 … 6.6)
RCA4/MPI-ESM-LR	1.9 mm d^{-1}	1.0 (0.44 … ∞)	−0.048 (−9.4 … 2.9)
RCA4/IPSL-CM5A-LR	1.5 mm d^{-1}	0.35 (0.12 … 2.6)	8.0 (−4.1 … 10)
RCA4/CSIRO-Mk3-6-0	0.90 mm d^{-1}	7.2 (1.5 … ∞)	−6.7 (−14 … −2.5)
RCA4/NorESM1-M	1.2 mm d^{-1}	3.8 (0.53 … ∞)	−3.5 (−14 … 3.3)
RCA4/GFDL-ESM2M	1.9 mm d^{-1}	4.3 (0.50 … ∞)	−4.5 (−8.3 … 3.6)
CCLM4-8-17/CNRM-CM5	1.2 mm d^{-1}	1.1 (0.91 … 1.4)	−0.73 (−2.2 … 0.66)
CCLM4-8-17/EC-EARTH	0.70 mm d^{-1}	2.0 (1.8 … 2.6)	−6.6 (−8.5 … −5.0)
CCLM4-8-17/HadGEM2-ES	0.70 mm d^{-1}	2.3 (1.4 … 3.2)	−6.0 (−7.7 … −2.4)
CCLM4-8-17/MPI-ESM-LR	0.90 mm d^{-1}	1.8 (0.59 … ∞)	−2.1 (−12 … 3.1)
HIRHAM5/EC-EARTH	1.4 mm d^{-1}	2.9 (1.8 … ∞)	−5.6 (−12 … −2.3)
RACMO22T/EC-EARTH	1.1 mm d^{-1}	1.4 (0.95 … ∞)	−2.1 (−10 … 0.27)
RACMO22T/HadGEM2-ES	1.3 mm d^{-1}	1.7 (1.0 … ∞)	−2.6 (−5.5 … −0.17)
REMO2009/EC-EARTH	1.7 mm d^{-1}	5.4 (0.36 … ∞)	−6.6 (−12 … 5.7)
REMO2009/HadGEM2-ES	1.7 mm d^{-1}	0.84 (0.51 … ∞)	1.4 (−12 … 4.0)
REMO2009/MPI-ESM-LR	1.8 mm d^{-1}	0.53 (0.33 … 59)	2.9 (−7.2 … 8.1)
REMO2009/IPSL-CM5A-LR	1.9 mm d^{-1}	1.1 (0.80 … ∞)	−0.50 (−8.2 … 1.8)
REMO2009/MIROC5	1.7 mm d^{-1}	3.5 (1.3 … ∞)	−6.6 (−12 … −1.6)
HadGEM3-GC31-HM HighresMIP	1.6 mm d^{-1}	3.8 (0.24 … 23)	−9.3 (−15 … 4.6)
EC-Earth3P-HR HighresMIP	1.8 mm d^{-1}	0.57 (0.000 22 … 2.2×10^2)	1.6 (−13 … 21)
MPI-ESM1-2-XR HighresMIP	1.9 mm d^{-1}	0.0084 (0.0018 … 1.6)	51 (−4.5 … 84)
GFDL/AM2.5C360	2.6 mm d^{-1}	0.19 (0.084 … 1.8)	8.8 (−3.2 … 13)
FLOR	1.8 mm d^{-1}	1.0 (0.47 … 4.3)	−0.064 (−6.0 … 3.3)

Figure 10. Scatter plot of the PR calculated with a 12 month precipitation index, relative to the default PR for the 24 month precipitation index. Results are presented for all CORDEX ensemble members (dots with numbers above corresponding to the model used), with their related uncertainties (coloured lines) and the ERA5 best-guess PR also shown. Black dashed lines denote a PR of 1.

The CORDEX models show a modest drying tendency for 24 month low-rainfall extremes, with a small majority of models showing a PR larger than 1. However, few of these models exhibit a significant drying trend, as was the case for the corresponding HiResMIP and GFDL multi-member ensembles.

As a brief sensitivity test, we also considered an alternative definition of the drought index (figure 10), analysing rainfall accumulations over a 12 month period (still July–June) instead of a 24 month period with the CORDEX-Africa ensemble. Of those 20 CORDEX models included in the 24 month analysis (where seven showed a best-guess PR at or below 1), only two have a corresponding (best-guess) PR below one when looking at 12 month precipitation deficits. However, it is stressed that the majority of these individual models which show a small increase in the likelihood of extreme dryness over 12 months also remain statistically insignificant.

6. Hazard synthesis

This section shows PRs and change in intensity (ΔI) for models, while also including the values calculated from the fits with observations. We synthesise the models with the observations to give an overarching attribution statement (please see e.g. Kew *et al* (2021) for details on the synthesis technique including how weighting is calculated for observations and for models).

Observations and models are combined into a single result in two ways. First, we neglect common model uncertainties beyond the averaged model spread that is depicted by the bright red bar, and compute the weighted average of models and observations: this is indicated by the magenta bar. The weighting applied is the inverse square of the variability (the width of the bright bars). Second, model uncertainty can be larger than the model spread because of common model uncertainties: we thus also show the more conservative estimate of an unweighted average of observations and models, indicated by the white box accompanying the magenta bar in the synthesis figures.

Figures 11 and 12 show the synthesis results for the current vs. past climate. For the intensity change (that is, the change in total rainfall associated with a 1-in-135 year drought when comparing the past and present climate), we report the weighted synthesis value. Where the results for the PR do not give a finite number we replace them by 10 000, to allow all models to be included in the synthesis analysis (sensitivity tests with alternative values yielded no effect on the final results (not shown)). This means that the reported synthesized PR gives a more conservative, lower value.

Results for current vs past climate, or for 1.2 °C of global warming vs pre-industrial conditions in 1850–1900, indicate a non-significant change in total rainfall associated with a 24 month drought like the one recently observed, of −2.1% (95% CI: −7.4%–3.8%). Note that a negative change in intensity means a shift towards drier extremes.

Results also show a non-significant PR of 1.36 (95% CI: 0.50–3.39), with values larger than one indicating a shift towards drier extremes. This means that if a 24 month drought event has a return period of 135 years in the current climate (as is our best estimate for the observed event), then an equivalent event would have a return period of 180 years in a pre-industrial climate, though uncertainty remains high and this latter number could range from as low as 70 years to as high as 450 years.

We conclude that even though models show, on average, a small increase of major 2 year droughts like the 2019–2021 one, the trend is not statistically significant compared to natural variability.

7. Discussion

A multitude of government policies and other measures exist to minimise drought-induced food insecurity in this region.

Madagascar is currently insured under the African Risk Capacity Insurance, with premiums paid in full by the African Development Bank (ARC 2021). It received its first payout of USD 2.13 million in July 2020 to support anticipated livelihood losses due to crop failure (AfDB 2020). A drought and food security early warning system (Système d'Alerte Precoce) was also established in 2005 to monitor food security in the Grand Sud, and it has changed administrators a number of times since (IFRC 2014). Different international agencies are supporting the government with early warnings, including the Food and Agriculture Organisation which publishes a report on food security and agriculture every quarter and ranks risks by their likelihood and potential impact (FAO 2019). Until last year, UNICEF worked with the Ministère de l'Eau, de l'Assainissement et de l'Hygiène to develop a monitoring system for the South in which bulletins were published every month, reporting on precipitation and Normalized Difference Vegetation Index (NDVI) anomalies based on CHIRPS and Moderate Resolution Imaging Spectroradiometer (MODIS) data compared to historical trends (UNICEF 2020).

Figure 11. Synthesis of PRs, when comparing the 2019–21 event with a pre-industrial climate.
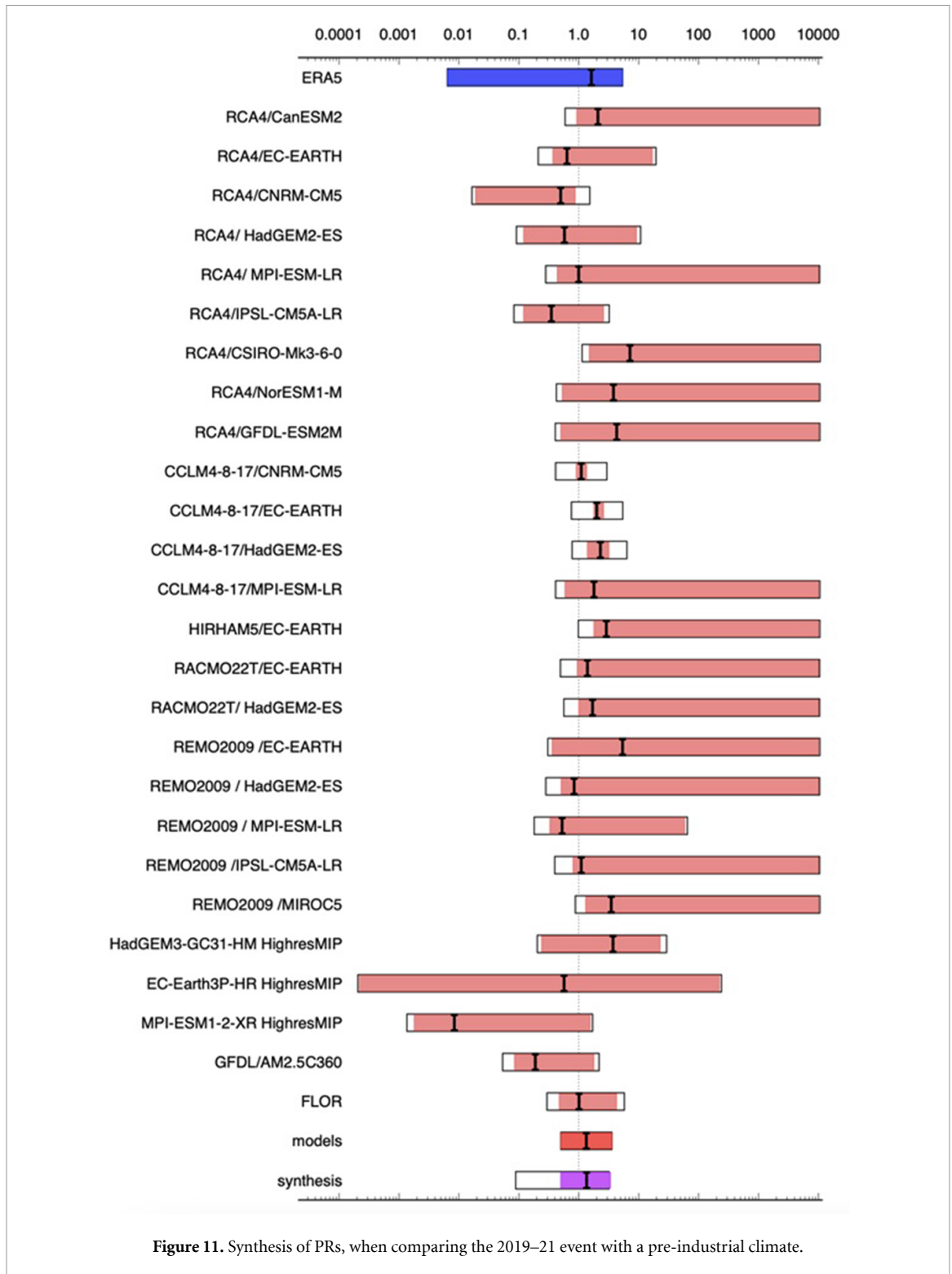
In 2015, the country adopted its first National Social Protection Policy (MPPSPF 2015). Under the national Social Protection policy, the government launched three main cash-transfer programmes: the cash-for work or Productive Safety Net programme, the Human Development Cash Transfer for families with young children, and the 'FIAVOTA' response for drought affected households (FID 2019). According to the World Bank (2021) these main cash-transfer programmes covered 2.5 million people (9% of the total population) between 2019 and 2021. However, certain barriers to the policies effectiveness have been highlighted in the literature, including fragmented cash-transfer programmes, low coverage, a lack of coordination, and low public expenditure to support the programmes (Rabi 2019). Efforts to increase the coherence of the system are underway (see Berrou *et al* 2021). In addition, the World Bank has provided three Grants intended to aid in development. The first was a March 2019 Grant of USD 90 million to support
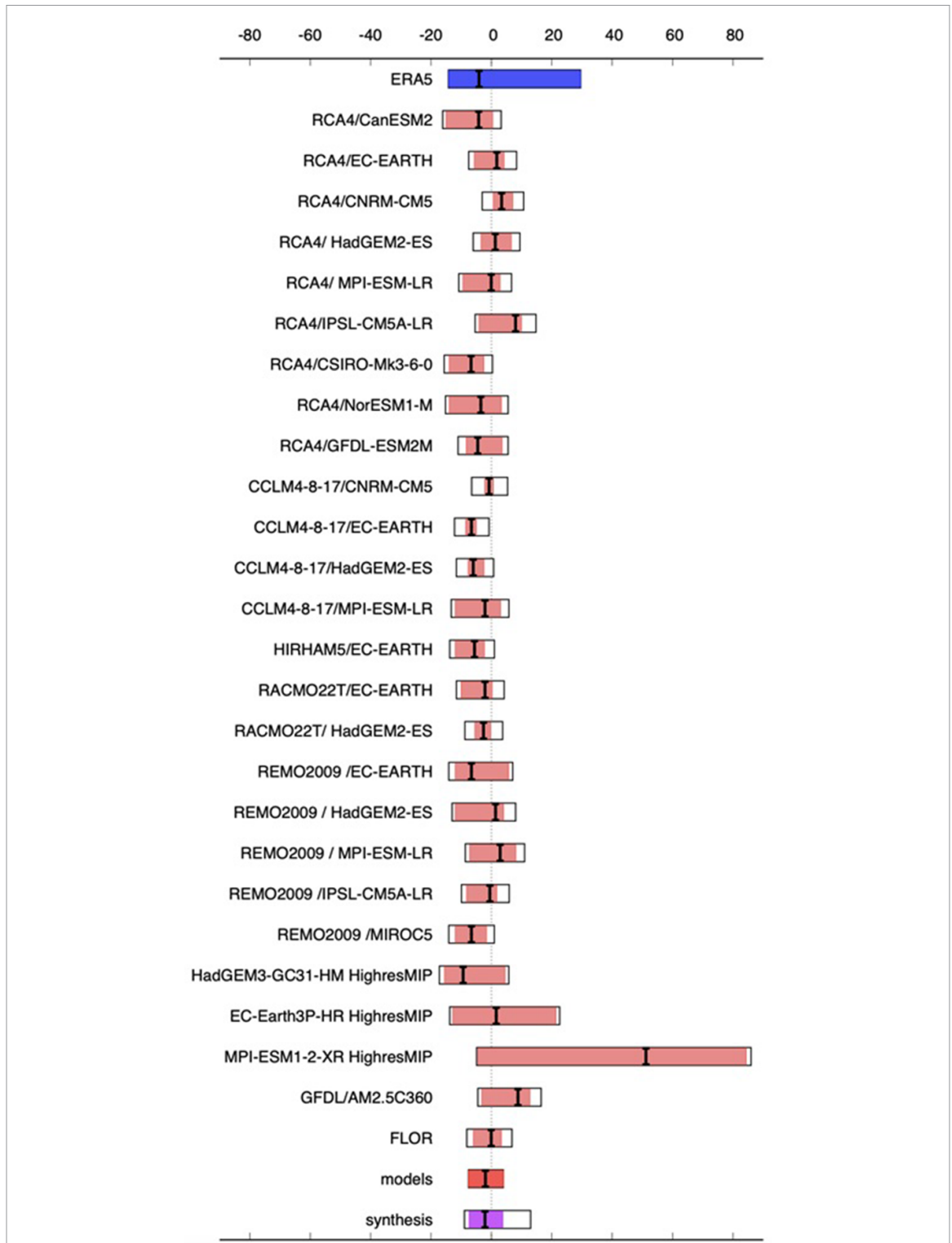
Figure 12. Synthesis figure, showing per cent changes in 24 month total rainfall, when comparing the 2019–21 event with an event of an equivalent return period in the pre-industrial climate.

the social safety programme (March 2019); the second was a USD 100 million Grant, approved in December 2020, to 'improve access to basic infrastructure and livelihood opportunities and strengthen local governance in southern Madagascar' (World Bank 2020b); the third was a March 2021 Grant of USD 150 million to further bolster the country's social safety programme, including the COVID-19 social protection response (World Bank 2021).

Finally, the government has a national drought contingency plan that activates based on the crossing of a threshold of emergency indicators such as comparative rainfall, food prices, water availability, social protection admissions and more (République de Madagascar 2021, Razanakoto 2017). However, the plan

focuses on drought and does not address the wider challenges of chronic food insecurity or other dimensions of vulnerability previously discussed in section 1.2.1.

7.1. Future outlook

In its September 2021 update on the food security situation in Southern Madagascar, FEWS NET projected that despite rainfall likely being near average in the October 2021 to May 2022 period, food insecurity will likely persist in the Grand Sud due to insufficient seed and cutting supplies from previous low-productivity seasons, average pest attacks made challenging by 'near zero' capacity for pest control, and a continued dearth of casual labour opportunities due to the COVID-19 pandemic (FEWS NET 2021b). This combination of factors underscores the complexity of food security in the region, as well as the difficulty to 'bounce back' following failed seasons, even if a rainy season is climatologically normal—or, indeed, even if rainy season failures are not yet occurring more often due to climate change.

8. Summary

The semi-arid climate of le Grand Sud is a challenging backdrop for subsistence farming, even in meteorologically 'normal' years. Vulnerability in this region is high due to, among other factors, the interplay of poverty, structural underinvestment in development, especially historically, and land use policies that have diminished pastoralist options. This backdrop has combined with a series of reduced rainfall years and the limitations posed by the COVID-19 pandemic, making a challenging situation worse. While climate change did not play a statistically significant role in the reduced rainfall that contributed to this current food crisis, as noted in other parts of this paper, the impacts currently being felt by the combination of hazard, vulnerability and exposure in this region are a warning sign for the future (Raju *et al* 2022). This also points to an opportunity to avert future harm: structural investments, such as those that are currently underway, have the potential to improve critical infrastructure, strengthen social protection systems and diversify livelihood opportunities. Investments such as these will become even more crucial if global warming continues at current rates. For example, should global warming exceed 2 °C, there is *medium confidence* that agricultural droughts may increase in frequency across Madagascar as a whole (IPCC AR6 2021). This could further increase risks of food insecurity, if the vulnerability of people and systems are not reduced.

Data availability statement

The data that support the findings of this study are openly available at the following URL/DOI: https://climexp.knmi.nl/MadagascarDrought2021.cgi.

Eulogy

Geert Jan van Oldenborgh passed away on 12 October 2021, part way through the completion of this analysis. He helped to define the event, analysed the observational data and also helped with framing the study. He is dearly missed not just for his wisdom, experience and integrity, but also as our friend and constant reminder why we do this. His contributions to the science of extreme weather event attribution were immense and will continue to influence us and many others as we continue to understand the effects of global warming on extreme weather.

Acknowledgments

ORCID iDs

Luke J Harrington ⓘ https://orcid.org/0000-0002-1699-6119
Rondrotiana Barimalala ⓘ https://orcid.org/0000-0001-7948-7699

Robert Vautard https://orcid.org/0000-0001-5544-9903
Lisa Thalheimer https://orcid.org/0000-0002-3737-3586
Sihan Li https://orcid.org/0000-0002-2479-8665
Remy Bonnet https://orcid.org/0000-0002-9267-674X
Wenchang Yang https://orcid.org/0000-0003-0053-9527
Friederike E L Otto https://orcid.org/0000-0001-8166-5917

References

Abram N J *et al* 2020 Coupling of Indo-Pacific climate variability over the last millennium *Nature* **579** 385–92

AfDB 2020 (available at: https://bit.ly/3NnJZ2A)

ARC 2021 (available at: www.arc.int/countries)

Barimalala R, Desbiolles F, Blamey R C and Reason C 2018 Madagascar influence on the South Indian Ocean convergence zone, the Mozambique Channel trough and Southern African rainfall *Geophys. Res. Lett.* **45** 11380–9

Barimalala R, Raholijao N, Pokam W and Reason C J C 2021 Potential impacts of 1.5 °C, 2 °C global warming levels on temperature and rainfall over Madagascar *Environ. Res. Lett.* **16** 044019

Beck H E, Zimmermann N E, McVicar T R, Vergopolan N, Berg A and Wood E F 2018 Present and future Köppen-Geiger climate classification maps at 1-km resolution *Sci. Data* **5** 180214

Benson C and Clay E 1998 *The Impact of Drought on Sub-Saharan African Economies* (Washington, DC: The World Bank)

Berrou J-P, Piveteau A, Deguilhem T, Delpy L and Gondard-Delcroix C 2021 Who drives if no-one governs? A social network analysis of social protection policy in Madagascar *SSRN Scholarly Paper No. ID 3811178* (Rochester, NY: Social Science Research Network) Retrieved from (available at: https://papers.ssrn.com/abstract=3811178)

Cai W, Yang K, Wu L, Huang G, Santoso A, Ng B, Wang G and Yamagata T 2021 Opposite response of strong and moderate positive Indian Ocean Dipole to global warming *Nat. Clim. Change* **11** 27–32

Chan D, Vecchi G, Yang W and Huybers P 2021 Improved simulation of 19th-and 20th-century North Atlantic hurricane frequency after correcting historical sea surface temperatures *Sci. Adv.* **7** eabg6931

Ciavarella A *et al* 2021 Prolonged Siberian heat of 2020 almost impossible without human influence *Clim. Change* **166** 9

Coppola E *et al* 2021 Climate hazard indices projections based on CORDEX-CORE, CMIP5 and CMIP6 ensemble *Clim. Dyn.* **57** 1293–383

Dosio A, Jones R G, Jack C, Lennard C, Nikulin G and Hewitson B 2019 What can we know about future precipitation in Africa? Robustness, significance and added value of projections from a large ensemble of regional climate models *Clim. Dyn.* **53** 5833–58

FAO 2015 The impact of disasters on agriculture and food security 1–54 (available at: www.fao.org/publications/card/en/c/fa17f187-9b92-439f-9952-1d6c13d14782/)

FAO, IFAD, UNICEF, WFP and WHO 2019 The State of Food Security and Nutrition in the World 2019 *Safeguarding against economic slowdowns and downturns* (Rome: FAO) (available at: www.fao.org/3/ca5162en/ca5162en.pdf)

Fauchereau N, Pohl B, Reason C J C, Rouault M and Richard Y 2009 Recurrent daily OLR patterns in the Southern Africa/Southwest Indian Ocean region, implications for South African rainfall and teleconnections *Clim. Dyn.* **32** 575–91

Favre A, Hewitson B, Lennard C, Cerezo-Mota R and Tadross M 2013 Cut-off lows in the South Africa region and their contribution to precipitation *Clim. Dyn.* **41** 2331–51

FEWS NET 2020a March 2020 (available at: https://fews.net/southern-africa/madagascar/key-message-update/march-2020)

FEWS NET 2020b April 2020 (available at: https://fews.net/southern-africa/madagascar/food-security-outlook-update/april-2020)

FEWS NET 2020f October 2020 (available at: https://fews.net/sites/default/files/documents/reports/Madagascar_Outlook_Oct2020_Final_EN_1.pdf)

FEWS NET 2021a June 2021 (available at: https://fews.net/southern-africa/madagascar/alert/june-10-2021)

FEWS NET 2021b September 2021 (available at: https://fews.net/southern-africa/madagascar)

FID 2019 (available at: www.fid.mg/wp-content/uploads/2019/01/03-Fiavota-Mid-term-Policy-Brief-En.pdf)

Funk C *et al* 2015 The climate hazards infrared precipitation with stations—a new environmental record for monitoring extremes *Sci. Data* **2** 150066

Haarsma R J *et al* 2016 High resolution model intercomparison project (HighResMIP v1.0) for CMIP6 *Geosci. Model Dev.* **9** 4185–208

Hänke H and Barkmann J 2017 Insurance function of livestock, farmers coping capacity with crop failure in southwestern Madagascar *World Dev.* **96** 264–75

Hansen J, Ruedy R, Sato M and Lo K 2010 Global surface temperature change *Rev. Geophys.* **48** 4

Hart N C G, Reason C J C and Fauchereau N 2013 Cloud bands over Southern Africa: seasonality, contribution to rainfall variability and modulation by the MJO *Clim. Dyn.* **41** 1199–212

Hart N C G, Washington R and Reason C J C 2018 On the likelihood of tropical–extratropical cloud bands in the South Indian convergence zone during ENSO events *J. Clim.* **31** 2797–817

Healy *et al* 2018 The deep south (available at: https://bit.ly/3oWVR1d)

Hersbach H *et al* 2020 The ERA5 global reanalysis *Q. J. R. Meteorol. Soc.* **146** 1999–2049

Hoell A, Funk C, Magadzire T, Zinke J and Husak G 2015 El Niño–Southern Oscillation diversity and Southern Africa teleconnections during Austral Summer *Clim. Dyn.* **45** 1583–99

Hoell A, Funk C, Zinke J and Harrison L 2017 Modulation of the Southern Africa precipitation response to the El Niño Southern Oscillation by the subtropical Indian Ocean Dipole *Clim. Dyn.* **48** 2529–40

IFRC 2014 Madagascar: country case study report—how law and regulation supports disaster risk reduction UNDP (available at: http://drr-law.org/resources/Madagascar-Case-Study.pdf)

IFRC 2021 The compound impact of extreme weather events and COVID-19 (available at: www.ifrc.org/media/49590)

IPC 2021 Madagascar: acute food insecurity and acute malnutrition situation April 2021 (available at: https://bit.ly/3kQsKeT) April 2022

IPCC 2021 Climate change 2021: the physical science basis. Contribution of working group I to the sixth assessment report of the intergovernmental panel on climate change ed V Masson-Delmotte *et al* (Cambridge University Press)

Jury M R 2016 Summer climate of Madagascar and monsoon pulsing of its vortex *Meteorol. Atmos. Phys.* **128** 117–29

Jury M R, Parker B A, Raholijao N and Nassor A 1995 Variability of summer rainfall over Madagascar: climatic determinants at interannual scales *Int. J. Climatol.* **15** 1323–32

Kendon E J, Stratton R A, Tucker S, Marsham J H, Berthou S, Rowell D P and Senior C A 2019 Enhanced future changes in wet and dry extremes over Africa at convection-permitting scale *Nat. Commun.* **10** 1794

Kew S F *et al* 2021 Impact of precipitation and increasing temperatures on drought trends in eastern Africa *Earth Syst. Dyn.* **12** 17–35

Klinman M G and Reason C J C 2008 On the peculiar storm track of TC Favio during the 2006–2007 Southwest Indian Ocean tropical cyclone season and relationships to ENSO *Meteorol. Atmos. Phys.* **100** 233–42

Lenssen N J L, Schmidt G A, Hansen J E, Menne M J, Persin A, Ruedy R and Zyss D 2019 Improvements in the GISTEMP uncertainty model *J. Geophys. Res.: Atmos.* **124** 6307–26

Lim Kam Sian K T C, Wang J, Ayugi B O, Nooni I K and Ongoma V 2021 Multi-decadal variability and future changes in precipitation over Southern Africa *Atmosphere* **12** 742

Macron C, Richard Y, Garot T, Bessafi M, Pohl B, Ratiarison A and Razafindrabe A 2016 Intraseasonal rainfall variability over Madagascar *Mon. Weather Rev.* **144** 1877–85

Manning C, Widmann M, Bevacqua E, Loon A F V, Maraun D and Vrac M 2018 Soil moisture drought in Europe: a compound event of precipitation and potential evapotranspiration on multiple time scales *J. Hydrometeorol.* **19** 1255–71

MPPSPF 2015 (available at: www.social-protection.org/gimi/gess/RessourcePDF.action?id=55763)

Nikulin G *et al* 2012 Precipitation climatology in an ensemble of cordex-Africa regional climate simulations *J. Clim.* **25** 6057–78

OCHA 2021 (available at: https://reliefweb.int/sites/reliefweb.int/files/resources/MDG_20210118_Grand_Sud_Flash_Appeal_English.pdf)

Padrón R S, Gudmundsson L, Decharme B, Ducharne A, Lawrence D M, Mao J, Peano D, Krinner G, Kim H and Seneviratne S I 2020 Observed changes in dry-season water availability attributed to human-induced climate change *Nat. Geosci.* **13** 477–81

Philip S *et al* 2020 A protocol for probabilistic extreme event attribution analyses *Adv. Stat. Climatol., Meteorol. Oceanogr.* **6** 177–203

Rabi 2019 (available at: http://amjad-rabi.com/wp-content/uploads/Madagascar_Final-2017.pdf)

Raju E, Boyd E and Otto F 2022 Stop blaming the climate for disasters *Commun. Earth Environ.* **3** 1–2

Ranasinghe R *et al* 2021 Climate change information for regional impact and for risk assessment *Climate Change 2021: The Physical Science Basis. Contribution of Working Group I to the Sixth Assessment Report of the Intergovernmental Panel on Climate Change* ed V Masson-Delmotte *et al* (Cambridge: Cambridge University Press)

Randriamahefasoa T S M and Reason C J C 2017 Interannual variability of rainfall characteristics over southwestern Madagascar *Theor. Appl. Climatol.* **128** 421–37

Randriamarolaza L Y A, Aguilar E, Skrynyk O, Vicente-Serrano S M and Domínguez-Castro F 2021 Indices for daily temperature and precipitation in Madagascar, based on quality-controlled and homogenized data, 1950–2018 *Int. J. Climatol.* **42** 265-288

Rayner N A, Parker D E, Horton E B, Folland C K, Alexander L V, Rowell D P, Kent E C and Kaplan A 2003 Global analyses of sea surface temperature, sea ice, and night marine air temperature since the late nineteenth century *J. Geophys. Res. Atmos.* **108** D14

Razanakoto T 2017 Analyse de la vulnerabilite a la secheresse des familles paysannes Tandroy *Unpublished Doctoral Thesis* (University of Antananarivo)

Reason C J C 2007 Tropical cyclone Dera, the unusual 2000/01 tropical cyclone season in the South West Indian Ocean and associated rainfall anomalies over Southern Africa *Meteorol. Atmos. Phys.* **97** 181–8

République D M 2021 (available at: www.presidence.gov.mg/actualites/informations/sociale/732-des-solutions-perennes-contre-la-secheresse-dans-le-sud.html)

Seneviratne S I *et al* 2021 Weather and climate extreme events in a changing climate *Climate Change 2021: The Physical Science Basis. Contribution of Working Group I to the Sixth Assessment Report of the Intergovernmental Panel on Climate Change* ed V Masson-Delmotte *et al* (Cambridge: Cambridge University Press)

Taylor K E, Stouffer R J and Meehl G A 2012 An overview of CMIP5 and the experiment design *Bull. Am. Meteorol. Soc.* **93** 485–98

UNICEF 2020 (available at: www.unicef.org/madagascar/rapports/bulletin-dalerte-s%C3%A9cheresse-du-grand-sud-de-madagascar-2020)

van Loon A F *et al* 2016 Drought in the Anthropocene *Nat. Geosci.* **9** 89–91

van Oldenborgh G J *et al* 2021 Pathways and pitfalls in extreme event attribution *Clim. Change* **166** 13

Vecchi G A *et al* 2014 On the seasonal forecasting of regional tropical cyclone activity *J. Clim.* **27** 7994–8016

World Bank 2017 (available at: https://documents1.worldbank.org/curated/en/587761530803052116/pdf/127982-WP-REVISED-deep-south-V27-07-2018-web.pdf)

World Bank 2020a (available at: www.worldbank.org/en/country/madagascar/overview)

World Bank 2020b (available at: www.worldbank.org/en/news/press-release/2020/12/10/world-bank-provides-100-million-to-support-resilient-livelihoods-in-the-south-of-madagascar)

World Bank 2021 (available at: www.worldbank.org/en/news/press-release/2021/03/10/madagascar-150-million-additional-financing-to-strengthen-the-national-social-protection-programs-and-accelerate-the-cov)

World Food Programme 2021 (available at: www.wfp.org/countries/madagascar)

Yang W, Hsieh T-L and Vecchi G A 2021 Hurricane annual cycle controlled by both seeds and genesis probability *Proc. Natl Acad. Sci.* **118** e2108397118